Automatic Generation of Surface Meshes for Right Ventricle with 1-to-1 Correspondence from Cine-MR Images

Yi Su[1], May-Ling Tan[1], Soo-Kng Teo[1], Chi-Wan Lim[1], Liang Zhong[2,3], Ru-San Tan[2,3]

[1]Institute of High Performance of Computing, A*STAR, Singapore
[2]National Heart Centre, Singapore
[3]Duke-NUS Graduate Medical School, Singapore

Abstract

We develop an automatic method to generate a set of 4D 1-to-1 corresponding surface meshes of the right ventricle (RV) which are motion registered over the whole cardiac cycle. The inputs are a set of 3D RV surface meshes at different phases of the cardiac cycle, each reconstructed independently from border-delineated MR images. To generate point correspondence, a template mesh is matched to the actual shape of the RV meshes in each of the time phases. This is done via a coarse matching phase and a fine matching phase. In the former, an initial rough matching between the template and the target is achieved using a radial basis function (RBF) morphing process. The feature points on the template and target meshes are automatically identified using a parameterization method. In the latter, a progressive mesh projection process is used to conform the rough estimate to fit the exact shape of the target. In addition, an optimization-based smoothing process is used to achieve superior mesh quality and continuous point motion. Eight healthy volunteers were recruited for MRI scanning and the algorithm was tested on the acquired data. It was observed that the algorithm took an average of approximately 70 seconds to complete. The maximum absolute deviation of the matched model from the original geometry was 0.187mm.

1. Introduction

In contrast to the left ventricle (LV), the anatomy of the right ventricle (RV) is relatively more complex and can vary significantly in patient cohort, such as patients with repaired tetralogy of fallot (rTOF). Many studies have shown that MRI is a superior approach to quantify 3D ventricular geometry and function [1-4], as compared to echocardiography [5], ventriculography [6] angiography [7] and indicator-dilution methods [8]. In patients with demonstrable severe pulmonary regurgitation (PR) and borderline RV function, serial MRI assessment becomes mandatory for timing of pulmonary valve replacement (PVR) [9]. However, few works have focused on 4D (i.e., 3D + time) geometrical modelling and motion reconstruction of the RV. A lack of a high quality 4D RV model limits the ability to effectively quantitate and compare measures of RV morphology and function for evidence-based medicine.

In this study, we aim to develop a computational method to generate a set of 4D meshes of the RV geometry over the whole cardiac cycle such that there is 1-to-1 mesh correspondence across all time frames. We approach this problem by treating the change in RV morphology as a combination of geometrical operations as well as mechanical deformation behavior. This allows a more realistic way of deriving RV wall motion. Achieving such 1-to-1 mesh correspondence is essential for downstream computational processing, such as shape analysis, motion analysis and finite element modelling.

2. Method

The input to our algorithm is a set of surface meshes representing the instantaneous shape of the endocardial surface of the RV. Each RV mesh represents the configuration at a particular time frame and is reconstructed from the delineated contours of the RV endocardium, as shown in Fig. 1. This contour-delineation could be performed manually or by a suitable image segmentation algorithm [10].

The RV mesh at each instant (or time frame) is partitioned into 13 segments based on the nomenclature described in [11]. This 13 segments form the basis to generate a set of feature points for each frame of the cardiac cycle. The 1-to-1 mesh matching process takes place in two stages. In the coarse matching stage, the mesh representing the first frame of the cardiac cycle is used as a template (i.e., Ω_0) and is mapped to the subsequent frames (i.e., Ω_i) of the cardiac cycle. The mapping is performed using a radial basis function (RBF) approach with progressive projection coupled with local smoothing to ensure robustness. The source RBF feature

points are selected by utilizing landmarks derived from the partitioning of the mesh at the first time frame; the corresponding RBF target feature points are selected by utilizing landmarks derived from the partitioning of the mesh at the time frame to be mapped to. In the fine matching stage, the morphed mesh of Ω_0 is progressively projected towards Ω_i. After each step of the projection, a strain-energy-based optimization method is used to smooth the mesh. An underlying Virtual Geometry engine is used to preserve the geometry. Using this approach, we generate a 4D RV mesh model of the RV with 1-to-1 point correspondence at every time frame.

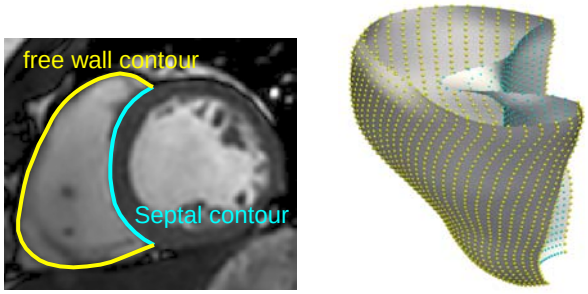

Figure 1. Reconstruction of RV mesh based on delineated contours of the RV endocardium.

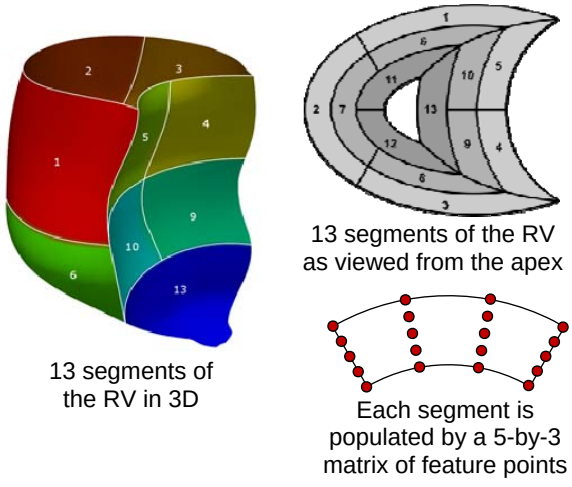

Figure 2. Partitioning of RV mesh into 13 segments.

2.1. Feature extraction from right ventricular models

Feature extraction of the RV is done via automatic mesh partitioning to generate landmarks for RBF morphing. The partitioning is based on the nomenclature described in [11]. Landmarks are extracted from each partition by selecting points on specific parametric positions on the patch representing each partition. Essentially, each segment is populated by a 5-by-3 matrix of feature points, as shown in Fig. 2. These form the set of feature points to be used for the RBF morphing.

2.2. Coarse matching using RBF morphing

Given two sets of n corresponding feature points $S = \{\mathbf{p}_i\} \subset \mathbb{R}^3$ and $T = \{\mathbf{q}_i\} \subset \mathbb{R}^3$ ($i = 1, \ldots, n$) that lie on the source mesh Ω_S and the target mesh Ω_T, respectively, we need to determine a function $\mathbf{f}$: $\mathbb{R}^3 \rightarrow \mathbb{R}^3$ such that

$$\mathbf{q}_i = \mathbf{f}(\mathbf{p}_i) + \mathbf{p}_i \qquad i = 1,\ldots,n \tag{1}$$

Radial Basis Functions (RBFs) are a popular means for interpolating scattered data for its ability to deal with irregular sets of data in multi-dimensional space in approximating high dimensional smooth surfaces [12]. Here, the interpolant is a function that returns the displacement value for each non-feature vertices of Ω_S and morphs them to the target shape. The displacements $\mathbf{u}_i = \mathbf{q}_i - \mathbf{p}_i$ are known for the source feature points $\mathbf{p}_i$ and the target feature points $\mathbf{q}_i$. These displacements are utilized to construct the interpolating function $\mathbf{f}(\mathbf{v})$ which returns the displacement for each mesh vertex $\mathbf{v}$. Such a mapping can be expressed by a weighted linear combination of n basic functions defined by the source feature points and an additional explicit affine transformation:

$$\mathbf{f}(\mathbf{v}) = \sum_{i=1}^{n} \mathbf{c}_i \phi(\|\mathbf{v} - \mathbf{p}_i\|) + \mathbf{R}\mathbf{v} + \mathbf{t} \tag{2}$$

where $\mathbf{v} \in \mathbb{R}^3$ is a vertex of Ω_S, $\mathbf{c}_i \in \mathbb{R}^3$ are (unknown) weights, ϕ is the radial basis function which is a real valued function on [0,1), $\|\cdot\|$ denotes the Euclidean norm, $\mathbf{R} \in \mathbb{R}^{3\times3}$ adds rotation, skew, and scaling, and $\mathbf{t} \in \mathbb{R}^3$ is a translation component. The RBF problem could be recast into a linear system which can then be solved using a standard LU decomposition with pivoting, hence obtaining the displacement vectors for all vertices of Ω_S.

2.3. Optimization-based mesh smoothing using Mooney-Rivlin strain energy function

The aim of the progressive mesh projection is to move Ω'_0 the morphed template mesh towards the desired target shape Ω_i in an iterative manner to preserve the validity of the mesh, e.g., that there are no inversion of elements. To do this, we use a ray-triangle intersection test to determine the propagation pathway of every vertex of Ω'_0 at every iteration. Essentially, we use the coordinates of each mesh vertex of Ω'_0 as the origin of a ray; we compute the normal vector at every vertex of Ω'_0 and use that as the ray vector; and we use Ω_i as the set of triangles to query for intersection.

To preserve the quality of the mesh during progressive

projection, we develop an optimization-based mesh smoothing method to improve the quality of the mesh during each iteration. The central idea is to consider the progressive projection process as a geometrical operation while treating the mesh smoothing as a strain-energy-minimization problem. As the coordinates of a mesh vertex is being modified in the direction of the ray, we compute the necessary correction to the vertex coordinates in the directions on the plane normal to the ray direction. By casting this as an energy-minimization problem, we can achieve a configuration that matches the geometrical configuration of the target, while achieving a mesh topology that reflects a realistic wall motion of the RV.

Here, we employ the Mooney-Rivlin Strain Energy Function [13], since the RV is a biological entity and is best described by a hyperlastic model. The strain energy density function (W) is given by

$$W = \frac{\mu}{2}(I_1 - 3) - \mu \ln(J) + \frac{\lambda}{2}\ln(J)^2 \quad (3)$$

where μ and λ are the Lame's constants, I_1 is the first invariants of the right Cauchy-Green deformation tensor C with $C = F^T F$ and F is the deformation gradient, J is determinant of the deformation gradients with $J = \det(F)$. The Green-Lagrangian strain tensor is denoted by $E = \frac{1}{2}(F^T F - \mathrm{I})$, where I is the identity matrix.

To compute the 2nd piola–kirchhoff stress tensor (S), we differentiate the strain energy density (W) with respect to the Green-Lagrangian strain tensor (E):

$$S = \frac{\partial w}{\partial E} = \mu(I - C^{-1}) + \lambda\{\ln(J)\}C^{-1} \quad (4)$$

The strain energy for the constant strain triangle (CST), denoted by U, is then computed by

$$U = \frac{1}{2} tA(E^{\mathrm{T}} S) \quad (5)$$

where t is the thickness of the CST (taken to be unity), and A is the area of the CST.

The 2nd piola–kirchhoff stress tensor (S) from the strain energy density function (W) is derived using chain rule

$$S = \frac{\partial W}{\partial E} = \frac{\partial W}{\partial C}\frac{\partial C}{\partial E} = \frac{\partial W}{\partial I}\frac{\partial I}{\partial C}\frac{\partial C}{\partial E} \quad (6)$$

Since $C = 2E + I, => \frac{\partial C}{\partial E} = 2.$ The strain energy density function W can be re-written as a function of the invariants of C in the following form

$$W = \frac{\mu}{2}(I_1 - 3) - \mu \ln\left(\sqrt{I_3}\right) + \frac{\lambda}{2}\ln\left(\sqrt{I_3}\right)^2 \quad (7)$$

where $I_3 = \det(C) = J^2$. This implies that

$$S = 2\frac{\partial W}{\partial I}\frac{\partial I}{\partial C} = 2\frac{\partial W}{\partial I_1}\frac{\partial I_1}{\partial C} + 2\frac{\partial W}{\partial I_3}\frac{\partial I_3}{\partial C} \quad (8)$$

And since $\frac{\partial I_1}{\partial C} = I$ and $\frac{\partial I_3}{\partial C} = I_3 C^{-1}$, so

$$S = 2\left(\frac{\mu}{2}\right)I + 2\left(I_3 C^{-1}\right)\left(-\mu\frac{1}{\sqrt{I_3}}\frac{1}{2\sqrt{I_3}} + \frac{\lambda}{2}2\ln(\sqrt{I_3})\frac{1}{\sqrt{I_3}}\frac{1}{2\sqrt{I_3}}\right) \quad (9)$$

Simplifying the above equation will lead to the final form of Equation (3).

The aim of the optimization is to minimize the strain energy function in Eqn. (5). We employ the L-BFGS-B algorithm [14] which is adept at solving multivariate nonlinear bound constrained optimization problems. Essentially, the algorithm aims to minimize a nonlinear objective function $F(\mathbf{x})$ of n variables, i.e.,

$$F(\mathbf{x}) \equiv F(x_1, x_2, x_3, ..., x_n) \quad (10)$$

The L-BFGS-B algorithm is based on the gradient projection method and uses a limited memory BFGS matrix to approximate the Hessian of the objective function $F(\mathbf{x})$. The gradient g_i associated with each variable x_i is defined as

$$g_i = \frac{F(x_1, ..., x_i + \Delta x_i, ..., x_n) - F(x_1, ..., x_i, ..., x_n)}{\Delta x_i} \quad (11)$$

where Δx_i is a small increment in x_i. Convergence of the optimization routine will result in a smoothed mesh configuration which has optimal mesh quality in terms of deformation.

3. Results

To test the algorithm, 17 human subjects were recruited. MRI scanning was performed using steady-state free precession cine gradient echo sequences on a 1.5 T Siemens scanner (Avanto, Siemens Medical Solution, Erlangen). The following planes were acquired: ventricular 2-chamber, 4-chamber, and short-axis planes with 12-14 equidistant slices covering both ventricles. The field of view was typically 320 mm with in-plane spatial resolution of <1.5 mm. Each slice was acquired in a single breath hold, with 22 temporal phases per cardiac cycle. The MRI data were processed using the CMRtools. Short- and long-axis images were displayed simultaneously such that segmentation of endocardial and epicardial contours in the two planes proceeded interactively to reduce registration errors. The segmentation was performed manually by a trained cardiologist for the end-diastole (ED) and end-systole (ES) phases. The papillary muscles were included in the chamber volume to obtain smooth endocardial contours. The 3D meshes created within CRMtools were used as inputs to our algorithm.

Our proposed method was implemented using C++ and the algorithm was tested on a workstation with an Intel Core i7-5960X CPU @ 3.00GHz, and 64Gb of RAM. Using our approach, we were able to achieve a 4D cardiac model with very high mesh quality in an automatic and robust manner. The motion of the time-series cardiac model were smooth and cyclical, and it took 70 ± 15.95

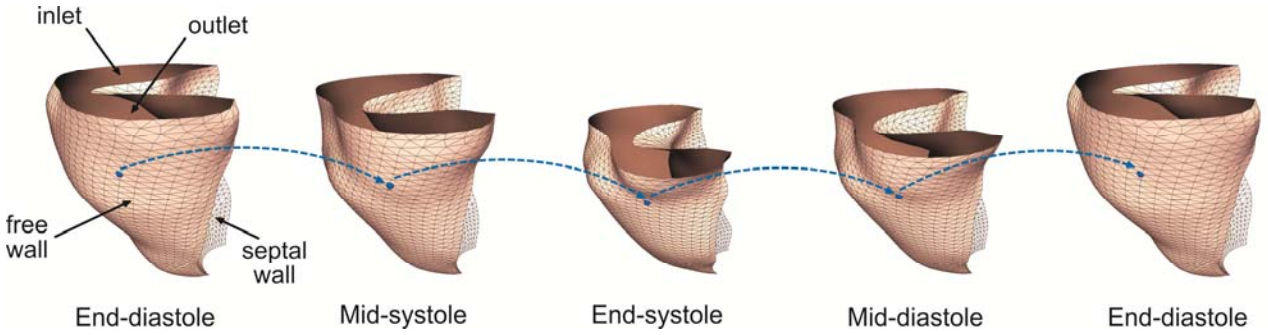

Figure 3. 4D cardiac model at selected time phases of the cardiac cycle. The blue dot shows the tracked position of a particular vertex over the cardiac cycle

seconds to generate the 1-to-1 corresponding 4D model.

4. Conclusion

We had designed and implemented a viable computational approach to automatically generate 1-to-1 mesh models of RV endocardial surfaces. The method had been successfully tested on 27 real human data extracted from cine-MR images and the computational performance suggests that real-time deployment in an actual clinical assessment pathway is possible. The availability of such a method will be beneficial to many new cardiac analysis methods that use 3D or 4D information, rather than the traditional 2D information.

References

[1] Bellenger NG, Francis JM, Davies CL, Coats A, Pennell DJ. Establishment and performance of a magnetic resonance cardiac function clinic. J Cardiovasc Magn Reson 2000; 2:15-22.

[2] Lessick J, Sideman S, Azhari H, Shapiro E, Weiss JL, Beyar R. Evaluation of regional load in acute ischemia by three-dimensional curvature analysis of the left ventricle. Ann Biomed Eng 1993; 21:147-161.

[3] Zhong L, Su Y, Yeo SY, Tan RS, Ghista DN, Kassab GS. Left ventricular regional wall curvedness and wall stress in patients with ischemic dilated cardiomyopathy. Am J Physiol Heart Circ Physiol 2009; 296: H573-H584.

[4] Zhong L, Su Y, Gobeawan L, Srikanth S, Tan RS, Kurra V, Navia JL, Ghista DN, Guccione J, Kassab G. Impact of surgical ventricular restoration on ventricular shape, wall stress and function in heart failure patients. Am J Physiol Heart Circ Physiol 2011; 300:H1653-H1660.

[5] Vogel M, Gutberlet M, Dittrich S, Hosten N, Lange PE. Comparison of transthoracic three dimensional echocardiography with magnetic resonance imaging in the assessment of right ventricular volume and mass. Heart 1997; 78: 127-130.

[6] Gaudio C, Tanzilli G, Mazzarotto P, Motolese M, Romeo F, Marino B, Reale A. Comparison of left ventricular ejection fraction by magnetic resonance imaging and radionuclide ventriculography in idiopathic dilated cardiomyopathy. Am J Cardiol 1991; 67:411-415.

[7] Semelka R, Tomei E, Wagners S, Mayo J, Kondo C, Suzuki J, Caputo G, Higgins C. Normal left ventricular dimensions and function: reproducibility of measurements with cine MR imaging. Radiology 1990; 174:763-768.

[8] Debatin J, Nadel SN, Sostman HD, Spritzer CE, Evans AJ, Grist TM. Magnetic resonance imaging-cardiac ejection fraction measurements. Phantom study comparing four different methods. Invest Radiol 1992; 27:198-204.

[9] Geva T. Repaired tetralogy of Fallot: the roles of cardiovascular magnetic resonance in evaluating pathophysiology and for pulmonary valve replacement decision support. J Cardiovasc Magn Reson 2011; 13:9.

[10] Yang XL, Yeo SY, Su Y, Lim C, Wan M, Zhong L, Tan RS. Right Ventricle Segmentation by Temporal Information Constrained Gradient Vector Flow. In: IEEE International Conference on Systems, Man 2013:13-16.

[11] Zhong L, Gobeawan L, Su Y, Tan JL, Ghista DN, Chua T, Tan RS, Kassab GS. Right ventricular regional wall curvedness and area strain in patients with repaired Tetralogy of Fallot. Am J Physiol Heart Circ Physiol. 2012; 302(6), H1306-H1316.

[12] Powell MJD. Radial basis functions for multivariate interpolation: A review. In: Mason JC, Cox MG, editors. Algorithms for Approximation. Clarendon Press, 1987:143-167.

[13] Shabana AA. Computational Continuum Mechanics, Cambridge University Press, 2008.

[14] Zhu CY, Byrd RH, Lu PH, Nocedal J. L-BFGS-B: Fortran Subroutines for large-scale bound constrained optimization. In: ACM Transactions on Mathematical Software (TOMS) 1997; 23(4):550-560.

Address for correspondence.

Yi Su
1 Fusionopolis Way, #16-16 Connexis, Singapore 138632.
suyi@ihpc.a-star.edu.sg